# A Low-cost Non-mechanical Maximum Power Point Tracking Scheme for Grid-tied Single-Phase Induction Generators

Rui Zhang, *Student Member, IEEE,* Faisal Khan, *Member, IEEE*
Department of Electrical and Computer Engineering, University of Utah
University of Utah
Salt Lake City, USA

***Abstract*—A new configuration of a single-phase induction generator based power generation system with maximum power point tracking capability is proposed in this paper, and this configuration is suitable for small-scale variable speed wind energy conversion system. Using this technique, the synchronous speed of the single-phase machine can be adjusted by regulating the frequency of the voltage applied at the auxiliary winding of the motor. Therefore, with variable electrical frequencies the maximum power can be extracted at different wind velocity. The steady-state model as well as the dynamic model of a single-phase induction generator is presented in order to analyze the system characteristics. In addition, a prototype of the system is implemented and tested. The experimental results have been presented and compared with simulation results to validate the peak power extracting capability. Using the proposed configuration, the generated power from the induction generator seems to be consistent with the available wind power.**

## I. INTRODUCTION

Wind power generators are becoming prevalent and have been widely employed both in stand-alone and grid-tied applications since their environment friendly characteristics. Among different kinds of electrical generators, induction generator could become the most suitable one for wind energy conversion system (WECS) because of its low cost, small footprint, robustness, high reliability and self protection against overload [1-2]. In addition, induction machines do not need the expensive rare earth materials. When a variable-pitch wind turbine including an induction generator is connected to a constant frequency grid, the induction generator operates at a speed closed to and a little higher than the synchronous speed of the motor. This kind of constant speed constant frequency (CSCF) operation leads to achieving low capture efficiency for wind energy, higher manufacturing cost and elevated complexity of the mechanical control [3]. However, the extracted power can be significantly improved if the wind turbine could work in varying shaft speed without any pitch control.

A great number of papers presenting the different configurations of induction generators with MPPT capacity exist in literature [2-7]. Reference [2] presented a squirrel-cage induction generator with a matrix converter which adjusts the induction generator's terminal frequency by adjusting the turbine shaft speed; and thus, it operates at the maximum power point (MPP). References [3-5] employed a wound rotor induction machine and a back-to-back converter to regulate the frequency of the applied voltage and the shaft speed. The stator of the machine has a direct grid connection, and the rotor is connected to the grid through the back-to-back converter. A wound rotor machine has decoupled stator and rotor frequency, and voltage/power control is much easier. However, wound rotor motors are difficult to manufacture and are terribly expensive. DC/DC converters with variable duty cycle are introduced in [6-7] for extracting the maximum power. The MPPT process is based on comparing the successive output power values by measuring the output voltage and current. All of these proposed configurations are suitable for three-phase induction generators, which are neither feasible nor cost effective for small-scale power generation units.

Several power generation units using a single-phase induction generator (SPIG) have been proposed in [8]. Fig. 1 shows a grid-parallel mode SPIG with a power electronic converter added between the grid and the auxiliary winding of the motor in order to control the voltage magnitude applied to the auxiliary winding of the motor, and this process eventually controls the reactive power flow to the auxiliary winding. The main disadvantage of this configuration is the requirement of shaft speed to be higher than the synchronous speed of the motor. The generator does not contribute any significant power at lower rotational speeds. Fig. 2 shows a configuration with a power converter added between the main winding and the grid in order to utilize the primary winding voltage and having variable voltage and frequency magnitudes. The main disadvantage of this configuration is the fixed capacitances across the main winding and the auxiliary winding. These

978-1-4577-1216-6/12/$26.00 ©2012 IEEE

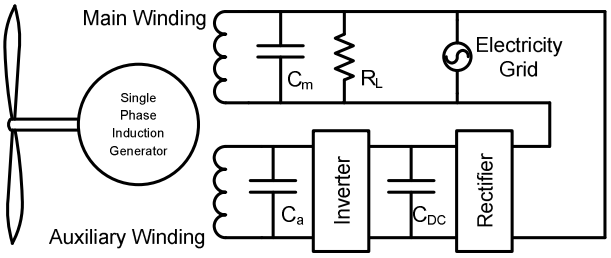


Figure 1. Schematic diagram 1 in reference [8].

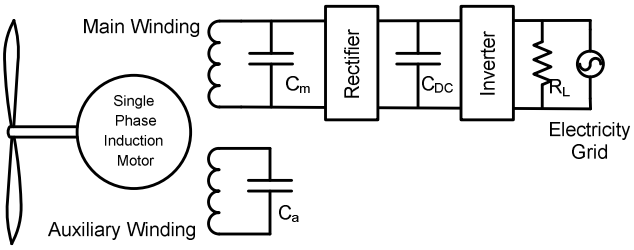


Figure 2. Schematic diagram 2 in reference [8].

capacitors may not guarantee a proper voltage regulation. More detailed description of the circuits and the summary of the characteristics can be found in [8]. Another drawback of these configurations is that these power generation units do not have the capacity to extract the maximum wind power. Their operating regions for power generation are narrow. A new configuration of a single-phase induction generator (SPIG) based power generation system with maximum power point tracking capability is proposed in section II. It enables the SPIG with maximum power point tracking capability to be operated in a wide range of the shaft speed. A dynamic as well as a steady-state model of an asymmetrical split phase induction motor have been introduced in section III for mathematical analysis. Section IV shows the simulation and experimental results in order to demonstrate the validity of this new configuration.

## II. System Description

In spite of having many favorable features, an SPIG produces reasonable electrical power only within a narrow operating range above the synchronous speed. Therefore, this phenomenon does not permit the application of SPIG in variable speed operation. However, the operational range of the generator can be expanded significantly by dynamically shifting the synchronous speed of the motor.

The proposed configuration is shown in Figure 3, which consists of a wind turbine, a single-phase squirrel-cage induction generator, and a power converter. There is no gearbox in the proposed system meaning the shaft speed of the wind turbine is the same as the rotational speed of the SPIG. The SPIG has two asymmetrical windings – the main winding and auxiliary winding. The proposed power converter scheme has two passive rectifiers and two inverter stages. Rectifier 1 and inverter 1 are inserted between the grid and the auxiliary winding of SPIG in order to supply variable voltage and frequency to the auxiliary winding. Rectifier 2 and inverter 2 are used to generate a 60 Hz voltage to be injected to the grid. The relationship between the main winding voltage and the auxiliary winding voltage depends on the applied rotational speed of the generator while the power consumed by the auxiliary winding remains zero. When the mechanical speed is high, the voltage produced from the main winding is higher than the one applied at the auxiliary winding, and vice versa. It is possible that the generated voltage from the main winding of the SPIG is lower than the grid voltage. Thus, a voltage doubler rectifier is needed for rectifier 2 in order to boost the dc bus voltage.

With the proposed configuration, the synchronous speed of this motor can be regulated by adjusting the frequency of the voltage applied to the auxiliary winding of the induction generator in form of $N_s = \frac{120 \times f}{P}$, where $N_s$ is the synchronous speed of the motor, $f$ is the frequency of the voltage supplied to the auxiliary winding of the SPIG, $P$ is the number of poles of the motor. Because it is a squirrel cage induction machine, the main and auxiliary winding voltages always have the same frequency. Furthermore, the

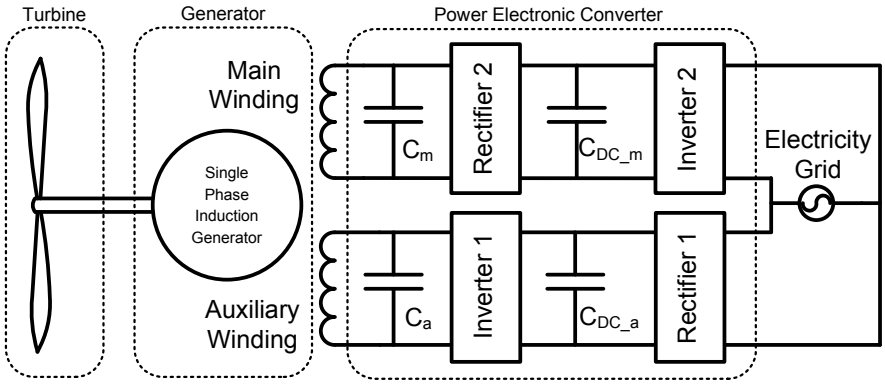


Figure 3. System level functional diagram of the proposed SPIG configuration.

synchronous speed of the SPIG can be adjusted with a minimum number of components (two capacitors, six diodes and eight transistors), and the output power can be optimized at various shaft speeds.

## III. System Modeling

The aerodynamic models of the wind turbine and the mechanical part (gear box) in wind energy conversion system are available in references [9-10], and many other models are available in literature. The maximum available electrical power is a function of the wind velocity and the shaft speed of the generator. This is a well researched area, and a huge number of models and technical papers are available. The concentration of this paper is to optimize the power converter scheme to extract power using an SPIG. However, conventional SPIG models could be used to design the system intended for the proposed MPPT operation.

For a four-pole and single-phase asymmetrical induction machine, the voltage equations can be obtained from the machine geometry. In order to obtain the voltage equations with constant coefficients, it is necessary to transform all machine variables to the stationary reference frame. Performing this transformation, the dynamic voltage and torque equations of an SPIG can be acquired as follows [8, 11].

$$v_{qs} = r_{qs} i_{qs} + p\lambda_{qs} \tag{1}$$

$$v_{ds} = r_{ds} i_{ds} + p\lambda_{ds} \tag{2}$$

$$0 = r'_{qr} i'_{qr} - n_p N_{qd} \omega_r \lambda'_{dr} + p\lambda'_{qr} \tag{3}$$

$$0 = r'_{dr} i'_{dr} + n_p N_{dq} \omega_r \lambda'_{qr} + p\lambda'_{dr} \tag{4}$$

$$T_e = p(N_{dq} \lambda'_{qr} i'_{dr} - N_{qd} \lambda'_{dr} i'_{qr}) \tag{5}$$

where

$$\lambda_{qs} = L_{lqs} i_{qs} + L_{mq}(i_{qs} + i'_{qr}) \tag{6}$$

$$\lambda_{ds} = L_{lds} i_{ds} + L_{md}(i_{ds} + i'_{dr}) \tag{7}$$

$$\lambda'_{qr} = L'_{lqr} i'_{qr} + L_{mq}(i_{qs} + i'_{qr}) \tag{8}$$

$$\lambda'_{dr} = L'_{ldr} i'_{dr} + L_{md}(i_{ds} + i'_{dr}) \tag{9}$$

$$p = \frac{d}{dt} \tag{10}$$

$$N_{qd} = \frac{1}{N_{dq}} \tag{11}$$

In these equations, $v_{qs}$ and $v_{ds}$ are the stator voltage in q-d axes, $r_{qs}$ and $r_{ds}$ are the stator resistance in q-d axes, $i_{qs}$ and $i_{ds}$ are the stator current in q-d axes, $\lambda_{qs}$ and $\lambda_{ds}$ are the stator flux linkage in q-d axes, $r'_{qr}$ and $r'_{dr}$ are the rotor resistance in q-d axes, $i'_{qr}$ and $i'_{dr}$ are the rotor current in q-d axes, $\lambda'_{qr}$ and $\lambda'_{dr}$ are the rotor flux linkage in q-d axes, $T_e$ is the electrical torque. Other parameters in the equations are: $n_p$ is the number of pole pairs, $N_{qd}$ is the turn ratio between q-axis and d-axis, $\omega_r$ is the rotational speed, $L_{lqs}$ and $L_{lds}$ are the stator inductance in q-d axes, $L'_{lqr}$ and $L'_{ldr}$ are the rotor inductance in q-d axes, $L_{mq}$ and $L_{md}$ are the mutual inductance in q-d axes.

In order to investigate the influence of supplied voltage frequency at windings, it is a convenient and effective way to express the voltage and flux linkages equations in terms of reactance rather than inductance. Because the relationship between inductance and reactance is $L = X/\omega_b$, the equations (1-4) and (6-9) above can be rewritten as:

$$v_{qs} = r_{qs} i_{qs} + \frac{p}{\omega_b}\varphi_{qs} \tag{12}$$

$$v_{ds} = r_{ds} i_{ds} + \frac{p}{\omega_b}\varphi_{ds} \tag{13}$$

$$0 = r'_{qr} i'_{qr} - n_p N_{qd} \frac{\omega_r}{\omega_b}\varphi'_{dr} + \frac{p}{\omega_b}\varphi'_{qr} \tag{14}$$

$$0 = r'_{dr} i'_{dr} + n_p N_{dq} \frac{\omega_r}{\omega_b}\varphi'_{qr} + \frac{p}{\omega_b}\varphi'_{dr} \tag{15}$$

where

$$\varphi_{qs} = X_{lqs} i_{qs} + X_{mq}(i_{qs} + i'_{qr}) \tag{16}$$

$$\varphi_{ds} = X_{lds} i_{ds} + X_{md}(i_{ds} + i'_{dr}) \tag{17}$$

$$\varphi'_{qr} = X'_{lqr} i'_{qr} + X_{mq}(i_{qs} + i'_{qr}) \tag{18}$$

$$\varphi'_{dr} = X'_{ldr} i'_{dr} + X_{md}(i_{ds} + i'_{dr}) \tag{19}$$

In equations (12-19), $X_{lqs}$ is the stator reactance in q-axis, $X_{lds}$ is the stator reactance in d-axis, $X'_{lqr}$ is the rotor reactance in q-axis, $X'_{ldr}$ is the rotor reactance in d-axis, $X_{mq}$ is the mutual reactance in q-axis, $X_{md}$ is the mutual reactance in d-axis, $\omega_b$ is the base electrical angular velocity used to calculate the inductive reactance. In this case $\omega_b = 2\pi f$, where $f$ is the auxiliary winding voltage frequency.

Applying the harmonics balance technique, the dynamic model of the SPIG can be converted to a steady-state model as follows:

$$V_{qsk} = [r_{qs} + j(X_{lqs} + X_{mq})]I_{qsk} + jX_{mq} I'_{qrk} \tag{20}$$

$$V_{dsk} = [r_{ds} + j(X_{lds} + X_{md})]I_{dsk} + jX_{md}I'_{drk} \quad (21)$$

$$0 = jX_{mq}I_{qsk} - n_p N_{qd}\frac{\omega_r}{\omega_b}X_{md}I_{dsk} + [r'_{qr} + (X'_{lqr} + X_{mq})]\times$$

$$I'_{qrk} - n_p N_{qd}\frac{\omega_r}{\omega_b}(X'_{ldr} + X_{md})I'_{drk} \quad (22)$$

$$0 = jX_{md}I_{dsk} + n_p N_{dq}\frac{\omega_r}{\omega_b}X_{mq}I_{qsk} + [r'_{dr} + (X'_{ldr} + X_{md})]\times$$

$$I'_{drk} + n_p N_{qd}\frac{\omega_r}{\omega_b}(X'_{lqr} + X_{mq})I'_{qrk} \quad (23)$$

Using these steady-state equations, the proposed configuration can be analyzed with different frequencies of the applied voltage. In order to simplify the analysis, a constant resistance load $R_L$ is connected to the main winding and a variable-frequency voltage source is attached to the auxiliary winding of the motor. The main winding voltage is $V_{qsk}$ and the voltage supplied to the auxiliary winding is $V_{dsk}$. Thus, another steady-state equation related with the power converter at the main winding can be obtained as:

$$V_{qsk} = -R_L C_m j\omega_{esk}V_{qsk} - R_L I_{qsk} \quad (24)$$

There are five unknown variables in (20-24). With three fixed variables, these steady-state equations can be solved, and the relationship between the other two variables can be acquired. This is an effective method to obtain the characteristics of the variable synchronous speed induction generator, and the relationships between the generated power and the operating speeds at different electrical frequencies are summarized and compared with experimental results presented in the next section.

## IV. Simulation and Experimental Results

The simulation model is implemented using Matlab® and the prototype of the SPIG system (shown in Figure 10) has been tested to verify the mathematical analysis and the simulation results. The nameplate ratings of the motor under test are listed in Table I. The capacitors $C_a$ and $C_m$ were set to 140 μF both in simulation and experiment.

TABLE I. Motor Characteristics

| Rating Power | Rating Voltage | Rating Frequency | Rating Speed |
|---|---|---|---|
| 250 W | 110 V | 60 Hz | 1800 RPM |

In order to acquire steady-state characteristics of the SPIG, equations (20-24) can be solved with different frequency of the voltage supplied to the auxiliary winding of the SPIG. The load resistor connected at the main winding is 50 ohms. The relationship between the rotational speed and the produced real power from the main winding can be obtained, which is shown in Figure 4. The generator produces a speed dependant active power, and separate characteristics can be obtained at different electrical frequencies. As a result, the maximum power can be tracked by adjusting the frequency of the voltage

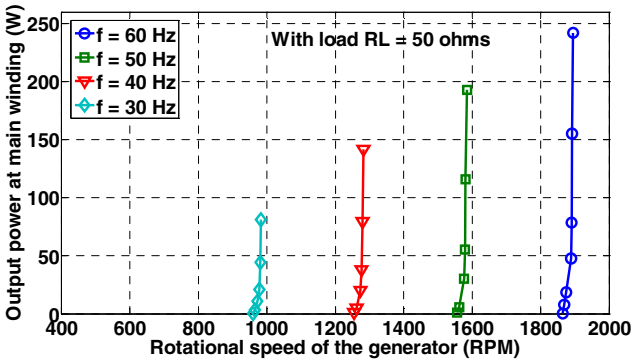


Figure 4. Relationship between rotational speed and the generated power from main winding at different electrical frequencies (**simulation results**).

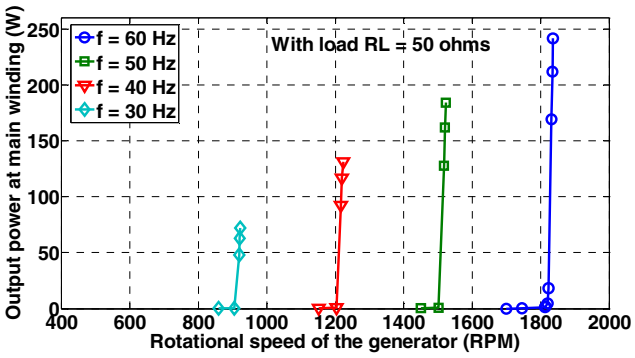


Figure 5. Relationship between rotational speed and the generated power from main winding at different electrical frequencies (**experimental results**).

applied at the auxiliary winding at various shaft speeds. A similar result is acquired from the experiment, and it is shown Figure 5. It can be seen from these results also that the operating range of the previous configuration (fixed 60 Hz electrical frequency) is narrow and is located above the synchronous speed of the motor. The generator cannot contribute any significant power when the rotational speed is lower than the synchronous speed.

Similarly, the simulation and experimental results for the schematic shown in Figure 2 can be obtained in Figure 6 and 7. During the test, capacitors $C_m$ and $C_a$ are connected at the main and auxiliary windings of the SPIG. With each pair of capacitors, the active power injected to the grid and the corresponding rotational speeds of the SPIG are recorded during the simulation and the experiment. Fig. 6 shows the simulation results of the active power supplied to the grid as a function of the rotational speed. A similar relationship obtained from the experiment is shown in Fig. 7. From the simulation and the experimental results, it is apparent that active power can be produced from the SPIG within a small range of mechanical speed with fixed capacitors. Furthermore, there is a rotational speed limitation for specific capacitors connected across the main and auxiliary windings. If the mechanical speed is lower than this minimum point, the main winding of the generator cannot produce any output voltage

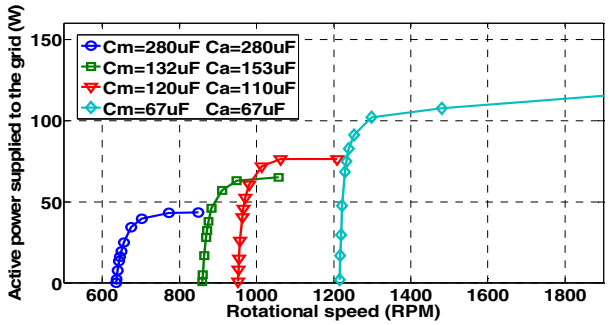


Figure 6. Simulation results of the active power supplied to the grid for the configuration shown in Figure 2.

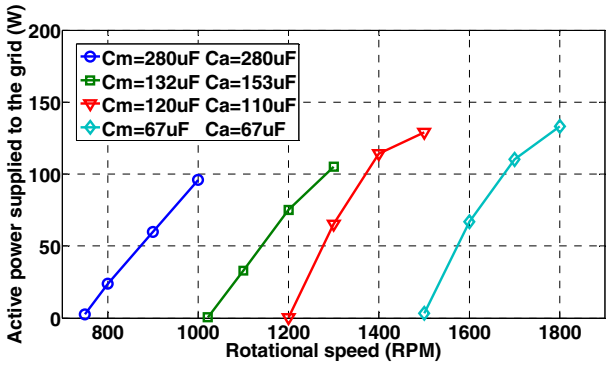


Figure 7. Experimental results of the active power supplied to the grid for the configuration shown in Figure 2.

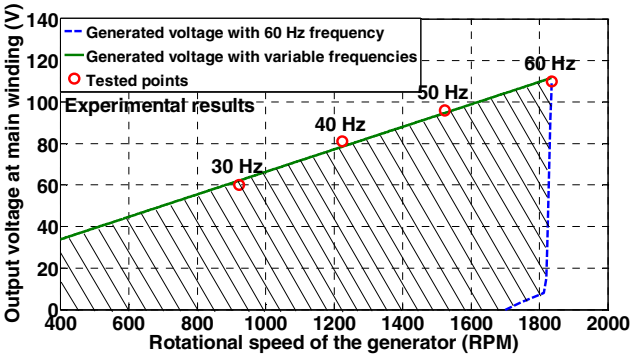


Figure 8. Shaft speed vs. generated voltage for MPPT.

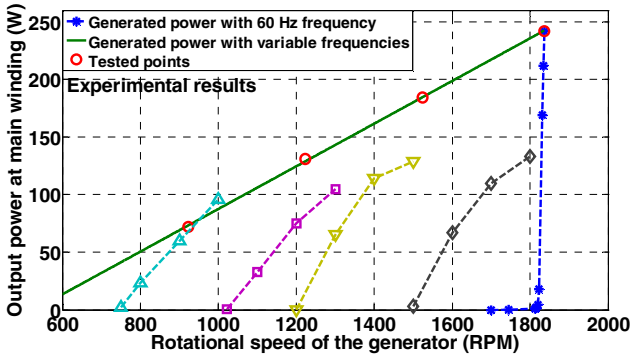


Figure 9. Shaft speed vs. produced power.

meaning the SPIG cannot enter into the self-excitation mode. Also, there is a maximum active power generation limit with fixed capacitors as well. If the rotational speed of the SPIG exceeds this point, the real power produced from the SPIG cannot increase any further. In order to produce active power from the SPIG within a wide operational range, an adjustable capacitor, such as capacitor bank is required. Moreover, larger capacitances are required at lower rotational speeds of the SPIG and smaller capacitors are needed at higher rotational speeds.

Therefore, the new configuration proposed in this paper is likely to improve the performance of the generation system. When the new configuration is connected to the grid, the dynamically controlled synchronous speed can be utilized for tracking the maximum power at any specific wind velocity. When the rotational speed of the generator decreases because of a smaller wind velocity, the available wind power declines as well. However, the available power can be maximized by decreasing the frequency supplied to the auxiliary winding of the motor. A reverse operation is needed for higher wind speed. Figure 8 shows the comparison between the generated voltages with fixed and variable electrical frequencies. The broken line indicates the relationship between the speed and the output voltage when a 60 Hz excitation is supplied to the auxiliary winding. The operational range of the generator with 60 Hz electrical frequency is considerably narrow. By contrast, the solid line shows the generated voltages with variable frequency control, and the operating range with frequency compensation could be extended significantly. The shaded area demonstrates increment in the produced voltage using the proposed configuration. Several key numerical values involved in this test are presented in Table II. Notice that at different mechanical speeds, the maximum power can be harnessed by regulating the frequency of the voltage applied at the auxiliary winding.

A comparison of power production among these three configurations is shown in Figure 9. It is obvious that the proposed configuration with MPPT can extract significantly higher energy from wind energy compared to the other two configurations. In addition, the power generated from the schematic shown in Figure 2 is higher than that from the schematic shown in Figure 3 because its operational range is much wider than the other one. However, a capacitor bank is needed for the self-excitation operation, which cannot guarantee the stability of the operating and the consecutive power generation. Thus, the proposed configuration is the best solution for SPIG.

TABLE II. TEST RESULTS AT DIFFERENT MECHANICAL SPEED AND ELECTRICAL FREQUENCY

| Electrical frequency | Rotational speed | Main winding voltage | Auxiliary winding voltage | Produced power at main winding |
|---|---|---|---|---|
| 60 Hz | 1836 RPM | 110 V | 108 V | 248 W |
| 50 Hz | 1524 RPM | 96 V | 115 V | 184 W |
| 40 Hz | 1223 RPM | 81 V | 101 V | 131 W |
| 30 Hz | 923 RPM | 60 V | 78.1 V | 72 W |

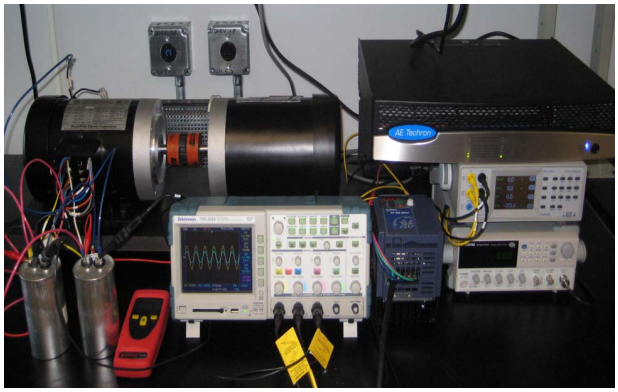

Figure 10. Experiments setup.

## V. CONCLUTIONS

A low-cost power generation scheme using single-phase induction generator with MPPT feature has been introduced in this paper. A conventional analytical model of asymmetric induction machine has been used to generate the simulation results, and the capability of the proposed configuration has been verified through the simulation and laboratory experiments. The experimental results have been presented and compared with the simulation results to verify the peak power extraction capability. In addition, experimental results obtained from the proposed configuration have been compared with two other previously developed solutions, and it is apparent that the power produced from the SPIG can be increased significantly by using the proposed configuration. In addition, the generated electrical power seemed to be consistent with the available wind power.

## REFERENCES


[1] R.C. Bansal, "Three-Phase Self-Excited Induction Generators: An Overview," IEEE Transactions on Energy Conversion, vol. 20, no. 2, pp. 292 - 299, 2005

[2] S.M. Barakati, M. Kazerani, J.D. Aplevich, "Maximum Power Tracking Control for a Wind Turbine System Including a Matrix Converter," IEEE Transactions on Energy Conversion, vol. 24, no. 3, pp. 705 - 713, 2009

[3] R. Datta, V.T. Ranganathan, "A method of tracking the peak power points for a variable speed wind energy conversion system," IEEE Transactions on Energy Conversion, vol. 18, no. 1, pp. 163 - 168, 2003

[4] Baike Shen, B. Mwinyiwiwa, Yongzheng Zhang, Boon-Teck Ooi, "Sensor less Maximum Power Point Tracking of Wind by DFIG Using Rotor Position Phase Lock Loop (PLL)," IEEE Transactions on Power Electronics, vol. 24, no. 4, pp. 942 – 951, 2009

[5] Wei Qiao, Wei Zhou, J.M. Aller, R.G. Harley, "Wind Speed Estimation Based Sensor less Output Maximization Control for a Wind Turbine Driving a DFIG," IEEE Transactions on Power Electronics, vol. 23, no. 3, pp. 1156 - 1169, 2008

[6] E. Koutroulis, K. Kalaitzakis, "Design of a maximum power tracking system for wind-energy-conversion applications," IEEE Transactions on Industrial Electronics, vol. 53, no. 2, pp. 486 - 494, 2006

[7] S.M.R. Kazmi, H. Goto, Hai-Jiao Guo, O. Ichinokura, "A Novel Algorithm for Fast and Efficient Speed-Sensor less Maximum Power Point Tracking in Wind Energy Conversion Systems," IEEE Transactions on Industrial Electronics, vol. 58, no. 1, pp. 29 - 36, 2011

[8] Rui Zhang, Faisal Khan, Marc Bodson, "Several Practical Configurations of a Grid-Tied Induction Generator Constructed from Inexpensive Single Phase Induction Motors", International Electric Machines and Drives Conference 2011, May 2011

[9] F. Blaabjerg, Zhe Chen, S.B. Kjaer, "Power electronics as efficient interface in dispersed power generation systems," IEEE Transactions on Power Electronics, vol. 19, no. 5, pp. 1184 - 1194, 2004

[10] S.M. Barakati, J.D. Aplevich, M. Kazerani, "Controller Design for a Wind Turbine System Including a Matrix Converter," IEEE Power Engineering Society General Meeting 2007, pp. 1 - 8, 2007

[11] Paul C. Krause, Oleg Wasynczuk, Scott D. Sudhoff, "Analysis of electric machinery and drive systems," IEEE Press, 2002